

## Mechanisms for the Advanced Asian Summer Monsoon Onset since the Mid-to-Late 1990s\*

BAOQIANG XIANG

*International Pacific Research Center, University of Hawaii at Manoa, Honolulu, Hawaii*

BIN WANG

*International Pacific Research Center, and Department of Meteorology,  
University of Hawaii at Manoa, Honolulu, Hawaii*

(Manuscript received 12 July 2012, in final form 21 September 2012)

### ABSTRACT

Understanding the variability and change of monsoon onset is of utmost importance for agriculture planning and water management. In the last three decades, the Asian summer monsoon onset (ASMO) has remarkably advanced, but the physical mechanisms underlying the change remain elusive. Since the overall ASMO occurs in May, this paper focuses on the change of mean fields in May and considers enhanced mean precipitation and monsoon westerly winds as signs of advanced ASMO. The results reveal that the advanced ASMO mainly represents a robust decadal shift in the mid-to-late 1990s, which is attributed to the mean state change in the Pacific basin characterized by a grand La Niña-like pattern. The La Niña-like mean state change controls the ASMO through the westward propagation of Rossby waves and its interaction with the asymmetric background mean states in the Indian Ocean and western Pacific, which intensifies the Northern Hemispheric perturbations and westerly winds. Intriguingly, the abrupt decadal shifts of monsoon onset in the Arabian Sea and Bay of Bengal occur in 1999, in contrast to the South China Sea with a decadal shift in 1994. Numerical experiments with a coupled climate model demonstrate that the advanced monsoon onset in the Arabian Sea and Bay of Bengal is governed by the enhanced zonal sea surface temperature (SST) gradients in the equatorial Pacific, while that in the South China Sea is primarily determined by the abrupt SST warming near the Philippine Sea.

### 1. Introduction

Since monsoon precipitation is the life blood of two-thirds of the world's population, its variability exerts tremendous impacts on agriculture, ecosystems, economics, and society in general. Meanwhile, an accumulation of evidence suggests that the monsoonal variability plays an essential role in affecting climate on a global scale. For example, the monsoon wind forcing in the western Pacific (WP) is strongly coupled to the

quasi-biennial oscillation (QBO) in the tropical ocean (Kim and Lau 2001). As a trigger factor, the Indian monsoon is argued to be able to enhance the El Niño–Southern Oscillation (ENSO) variability (Kirtman and Shukla 2000). The Indian monsoon can also extend its influences to the midlatitude climate through the so-called circumglobal teleconnection (CGT) (Ding and Wang 2005; Ding et al. 2011). In addition, monsoon variability acts as a significant source of extratropical climate predictability (Wang et al. 2009; Lee et al. 2010, 2011).

Extensive studies have been conducted to understand the interannual variability of the monsoon system, especially its relationship with ENSO variability, for several decades now (e.g., Webster and Yang 1992; Wang et al. 2000; Kumar et al. 2006), while studies on decadal and long-term trend variability of monsoon have been booming (e.g., Hu 1997; Kwon et al. 2007; Zhou et al. 2008; Hsu et al. 2011; Wang et al. 2012a). Several recent

---

\* School of Ocean and Earth Science and Technology Contribution Number 8756 and International Pacific Research Center Contribution Number 915.

---

Corresponding author address: Baoqiang Xiang, Post 401, 1680 East-West Rd., Honolulu, HI 96822.  
E-mail: baoqiang@hawaii.edu

studies have investigated the observed monsoon change from a global perspective and reported that both global monsoon precipitation and area demonstrate significant increasing trends in the most recent three decades (Hsu et al. 2011; Wang et al. 2012a). The future projections based on Intergovernmental Panel on Climate Change (IPCC) climate models also predict intensified global monsoon precipitation in the twenty-first century under global warming (Hsu et al. 2012; Lee and Wang 2013). However, Wang et al. (2012a) argued that the recent global monsoon variability is tightly linked to the mean state change in the Pacific basin, which primarily reflects the contribution from natural decadal variability.

In addition to the monsoon variability in the summertime, understanding the change in monsoon seasonal cycle is another interesting and critical issue. In particular, the monsoon onset change has important implications for agriculture planning, such as crop selection, planting, and irrigation. Recently, Kajikawa et al. (2012) revealed a salient advance of Asian summer monsoon (ASM) onset (ASMO) in the most recent three decades by comparing the epochal difference between 1994–2008 and 1979–93, finding that the monsoon onset advanced by about 2–4 pentads in the Bay of Bengal (BoB), Indochina Peninsula, and South China Sea (SCS) (Fig. 3 in Kajikawa et al. 2012). Some other studies noticed some similar features of monsoon onset on a regional basis (e.g., Wang et al. 2012b; Yu et al. 2012a; Kajikawa and Wang 2012). For example, the Arabian Sea (ArS) has experienced a considerable advance of monsoon onset that is perceived to be responsible for the tropical storm intensification during the monsoon developing period after year 1997 (Wang et al. 2012b); and Yu et al. (2012a) revealed a clear advance of monsoon onset in the BoB in the recent three decades, with 2009 as the earliest onset year. The SCS also exhibits significant decadal variability with advanced monsoon onset after 1993/94 (Kajikawa and Wang 2012).

One fundamental question arises, however: What causes this observed advanced ASMO? The advanced BoB monsoon onset was proposed to be forced by the change of the maximum sea surface temperature (SST) warming over the central BoB and the associated the first branch of northward propagating intraseasonal oscillation before its onset (Yu et al. 2012a,b). Kajikawa and Wang (2012) suggested that the abrupt advance of SCS monsoon onset after 1993/94 is related to the SST warming in the WP; Kajikawa et al. (2012) and Wang et al. (2012b) argued that the advanced ASMO is possibly governed by the enhanced heat contrast between Asian continent and the tropical Indian Ocean (IO). In this study, we investigate the ASMO by focusing on three contiguous seas (ArS, BoB, and SCS) and attribute the

recent advance of ASMO to the decadal mean state change in the Pacific since the mid-to-late 1990s.

This paper is organized as follows. Section 2 describes the data, methodology, and model experiments. Section 3 discusses the observational features of the advanced ASMO. In section 4, we use numerical experiments to elaborate physical mechanisms controlling the advanced ASMO. Section 5 explores the nature of the observed advance of ASMO and attributes it to natural decadal variability. The main findings and discussion are presented in section 6.

## 2. Data, methodology, and model experiments

### a. Observed data and methodology

Several monthly datasets are used in this study: 1) SST data from the National Oceanic and Atmospheric Administration (NOAA) Extended Reconstructed SST (ERSST v3b; Smith et al. 2008) from 1979 to 2011; 2) precipitation data from the Global Precipitation Climatology Project (GPCP, v2.2; Adler et al. 2003) from 1979 to 2010; 3) the interim European Centre for Medium-Range Weather Forecasts (ECMWF) Re-Analysis (ERA-Interim; Dee et al. 2011) data from 1979 to 2011; 4) the 40-yr ECMWF Re-Analysis (ERA-40; Uppala et al. 2005) data from 1958 to 2002; 5) the National Centers for Environmental Prediction (NCEP)–National Center for Atmospheric Research (NCAR) reanalysis (NCEP-1 henceforth; Kalnay et al. 1996) from 1948 to 2011; 6) the NCEP–Department of Energy (DOE) AMIP-II Reanalysis products (NCEP-2 henceforth; Kanamitsu et al. 2002) from 1979 to 2011; and 7) the Wave- and Anemometer-Based Sea Surface (10 m) Wind (WASWind) based on ship observations of wind speed and wind wave height archived in the International Comprehensive Ocean–Atmosphere Dataset (ICOADS) from 1950 to 2009 (Tokinaga and Xie 2011).

Two statistical methods are used to test the significance of trend and abrupt decadal shift. The first is a trend-to-noise test to examine the significance of the trend for various fields (Woodward and Gray 1993). The second is the Lepage test to detect the significance of an abrupt change (Lepage 1971; Yonetani 1992). This test judges the significance of discontinuity according to the sum of the squares of the normalized Wilcoxon and Ansari–Bradley statistics (Lepage 1971).

### b. Description of models and experiments

Two models are used in this study to examine the physical mechanisms for the advanced ASMO. The first model is a newly developed atmosphere–ocean coupled model—POP-OASIS-ECHAM Model (POEM) (Xiang

et al. 2012). This model couples the Parallel Ocean Program (POP; v2.0.1) ocean model (Smith et al. 1992) and ECHAM (v4.6) atmospheric model (Roeckner et al. 1996) via the Ocean–Atmosphere–Sea Ice–Soil (OASIS, v3.0) coupler (Valcke et al. 2003). The air–sea coupling region is within the latitudes between 60°S and 60°N. Beyond this region, the climatological SST and sea ice are prescribed. The resolution for the atmospheric model is T42 (about 2.8° in horizontal direction) with 19 vertical levels. The ocean model has 100 (zonal)  $\times$  116 (meridional) grid points and 25 vertical layers. The meridional resolution for the ocean model in the near-equatorial region is about 0.6°. More details about this model are given in Xiang et al. (2012).

As a common problem of current climate models, POEM also suffers excessive cold tongue extension and warm SST bias in the southeast Pacific associated with the spurious double intertropical convergence zone (ITCZ) (Xiang et al. 2012). Considering the fact that mean SST bias may alter the anomalous remote impacts in response to the equatorial Pacific SST forcing, here we utilize an annual mean SST correction in the SST equation. The correction is only constrained in the equatorial Pacific and southeast Pacific (not shown). The SST correction term is estimated by inversely fitting model SST tendency to observational climatology with the nudging method, and thus a long-term annual SST correction term can be obtained. We then add this term to the SST equation to perform the control run (CTRL). To demonstrate the potential influences of Pacific mean state change on the ASMO, four sensitivity experiments are further conducted by adding additional SST nudging in the

TABLE 1. Experiments conducted in the study (20 ensembles for each experiment). For the four sensitivity experiments (TROP, TROP\_warm, TROP\_cold, WNP\_warm), the initial state on 1 January is from CTRL for each ensemble.

Experiments	Description
CTRL	With annual cycle of SST correction in the equatorial Pacific and southeast Pacific.
TROP	Similar to CTRL but with a SST nudging in the tropical Pacific from January (contours in Fig. 8a).
TROP_warm	Similar to TROP but only with a SST warming nudging in the tropical western Pacific from January (contours in Fig. 9a).
TROP_cold	Similar to TROP but only with a SST cooling nudging in the tropical central eastern Pacific from January (contours in Fig. 9c).
WNP_warm	Similar to CTRL but with a SST warming nudging in the western North Pacific from January (Fig. 10a).

tropical Pacific or the western North Pacific (WNP) (Table 1). For each experiment, 20 ensembles are performed.

The second model we used is an intermediate 2.5-layer atmospheric model (Wang and Li 1993). The advantage of using this intermediate model is to easily isolate the relative contributions from different physical processes. This model integrates a Lindzen–Nigam-type boundary layer (Lindzen and Nigam 1987) with a first baroclinic Gill-type free troposphere (Gill 1980). The boundary layer and the free lower troposphere are strongly coupled with each other. On the one hand, the boundary circulation can be altered by free tropospheric heating via changing the geopotential height

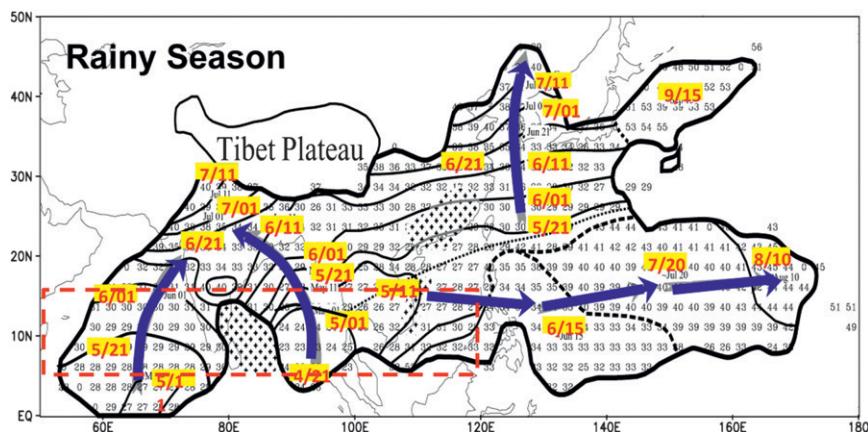


FIG. 1. Onset date of the Asian summer monsoon (ASM). The thick dashed line shows discontinuities (merger of three or more contours). The arrows point to the directions of rainbelt propagation. The thin dashed line divides subtropical monsoon and oceanic monsoon regions [modified from Fig. 6 in Wang and LinHo (2002)]. The red dashed-line rectangle outlines the domain we are focused on where the monsoon onset dates are mainly in May.

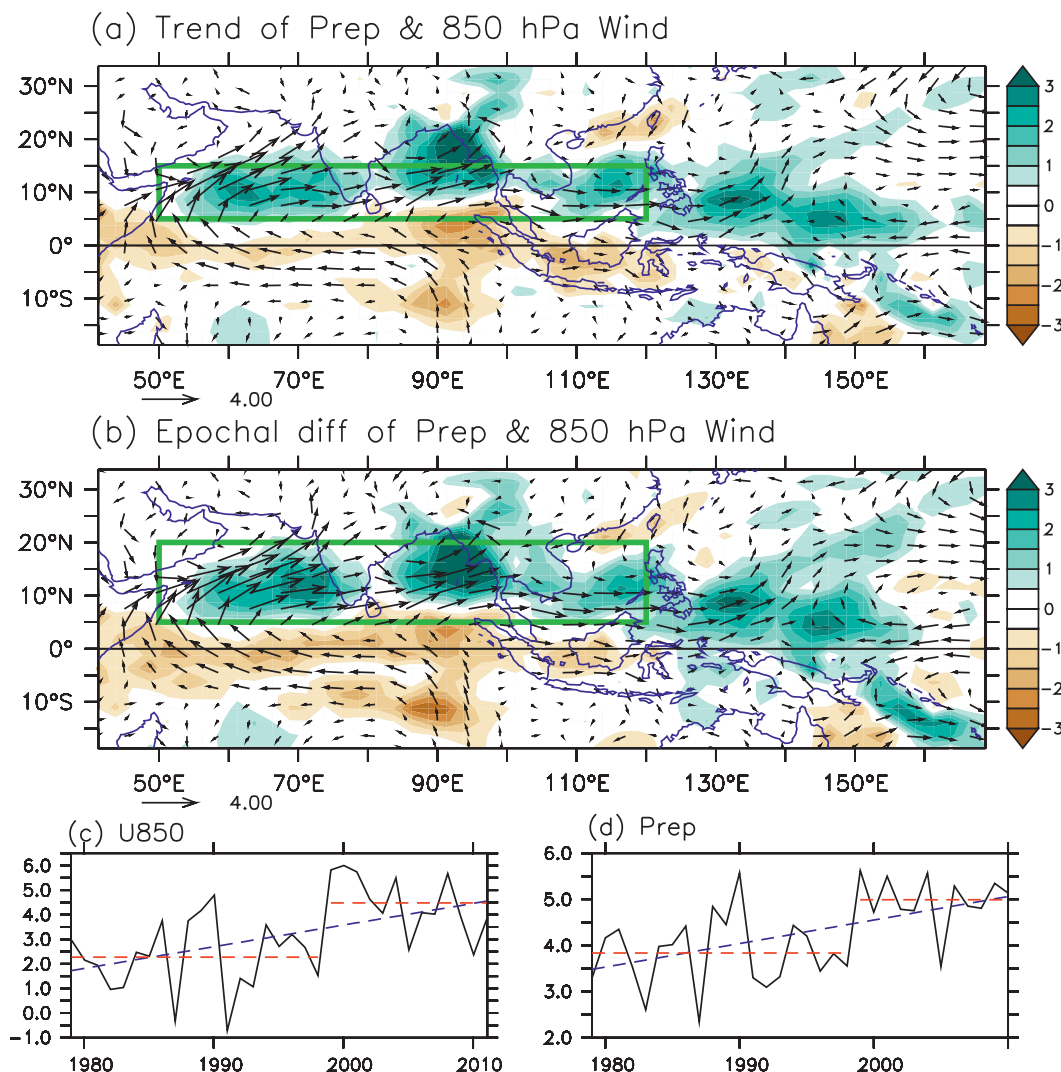


FIG. 2. (a) Monthly mean precipitation trend [ $\text{mm day}^{-1} (20 \text{ yr})^{-1}$ ] and 850-hPa winds trend [ $\text{m s}^{-1} (20 \text{ yr})^{-1}$ ] in May during the recent three decades. (b) Epochal differences of precipitation ( $\text{mm day}^{-1}$ ) and 850-hPa winds ( $\text{m s}^{-1}$ ) between post-1999 and pre-1999. (c) The 850-hPa zonal winds ( $\text{m s}^{-1}$ ) [U850 averaged over  $5^{\circ}$ – $15^{\circ}\text{N}$ ,  $50^{\circ}$ – $120^{\circ}\text{E}$ , green box in (a)]. (d) As in (c), but for precipitation ( $\text{mm day}^{-1}$ ) [averaged over  $5^{\circ}$ – $20^{\circ}\text{N}$ ,  $50^{\circ}$ – $120^{\circ}\text{E}$ , green box in (b)]. These two ASMO indices both show significant linear trend (above 95% confidence level based on trend-to-noise ratio test), and significant abrupt decadal shift at 1999 (above 99% confidence level based on the Lepage test). The wind (precipitation) data used here are from 1979–2011 (1979–2010) because of data availability. Correlation between the indices in (c) and (d) is 0.83 during 1979–2010.

at the top of the boundary layer. On the other hand, the tropospheric diabatic heating is largely influenced by the large-scale boundary moisture convergence. The presence of this feedback prompts the development of anomalous convection associated with convective instability.

### 3. Observed advance of ASMO in recent decades

Monitoring and determining the monsoon onset are mainly based on the seasonal march of precipitation and

circulation. Ramage (1972) first proposed to define the monsoon onset according to the annual reversal of surface winds. In the ASMO region, different criteria and definitions have been posed to determine the ASMO date (e.g., Tao and Chen 1987; Tanaka 1992; Murakami and Matsumoto 1994; Lau and Yang 1997; Wu and Wang 2001). This diversity of definitions poses a major hurdle to understand the monsoon variability on various time scales. Wang and LinHo (2002) put forward universal and objective criteria to describe the monsoon onset delineated by the relative pentad mean rainfall rate

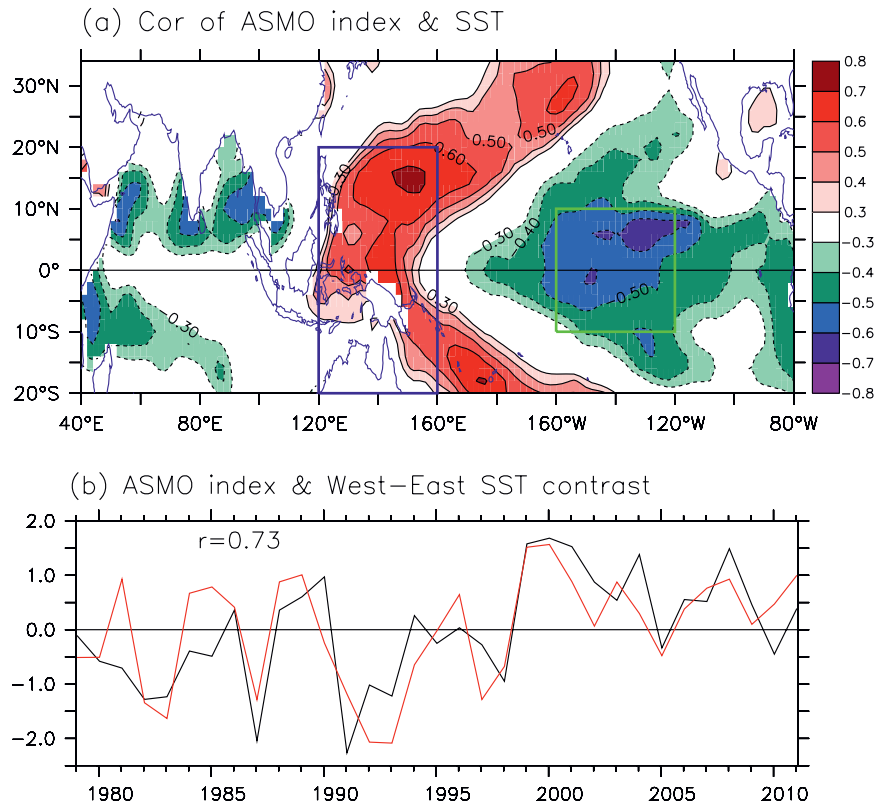


FIG. 3. (a) The correlation map between ASMO index (U850 averaged over  $5^{\circ}$ – $15^{\circ}$ N,  $50^{\circ}$ – $120^{\circ}$ E) and SST in May. Values with significance above 90% confidence level are shown. (b) The normalized ASMO index (black line) and the zonal [blue box – green box in (a)] SST gradients (red line) in May.

exceeding  $5 \text{ mm day}^{-1}$  compared with the January mean rainfall. Based on this, the earliest ASMO of rainy season is found to occur in the southeast BoB in late April (pentads 23–24), together with monsoon westerlies burst in the north equatorial IO. After that, the monsoon onset extends northeastward rapidly, passing over the Indochina Peninsula in early May (pentads 25–26), and then over the SCS in mid-May (pentads 27–28) (Fig. 1). In the ArS, the monsoon onset starts from the mid-May from the equatorial IO and then migrates northward, reaching the Indian subcontinent at the end of May (Fig. 1).

Since the ASMO in the studied domain (ArS, BoB, and SCS) mainly occurs during May (Fig. 1), hereinafter we focus on the change of monthly mean fields in May, which can be good surrogates to represent the variability of ASMO.

#### a. Features of observed ASMO in recent decades

Based on the criteria proposed by Wang and LinHo (2002), Kajikawa et al. (2012) quantitatively measured the ASMO change and found a dramatic advance of the ASMO in the last three decades. Similarly, we plot the linear trend of precipitation and 850-hPa winds in May

by using GPCP precipitation and ERA-Interim 850-hPa wind datasets (Fig. 2a). The trend pattern is manifested as a zonal band of enhanced precipitation from the northern IO to the equatorial WNP, accompanied by suppressed precipitation over the equatorial IO. A dynamical coherent wind pattern is observed, with easterly trend in the equatorial IO and westerly trend from the ArS to the equatorial WNP (Fig. 2a). Considering the zonally elongated patterns of 850-hPa winds and precipitation, we define two ASMO indices, 850-hPa zonal winds (U850, averaged over  $5^{\circ}$ – $15^{\circ}$ N,  $50^{\circ}$ – $120^{\circ}$ E) and precipitation (averaged over  $5^{\circ}$ – $20^{\circ}$ N,  $50^{\circ}$ – $120^{\circ}$ E) in May, to approximately represent the variability of ASMO (Figs. 2c,d). Although these indices cannot determine the accurate onset date, their interannual and decadal variabilities are highly indicative of ASMO variability.

With respect to these two indices, a trend-to-noise ratio test is employed to determine their statistical significance. Results show that their trends are both statistically significant with 99% of confidence level (Figs. 2c,d). Meanwhile, the features of these two indices also suggest robust decadal shifts in 1999, which is

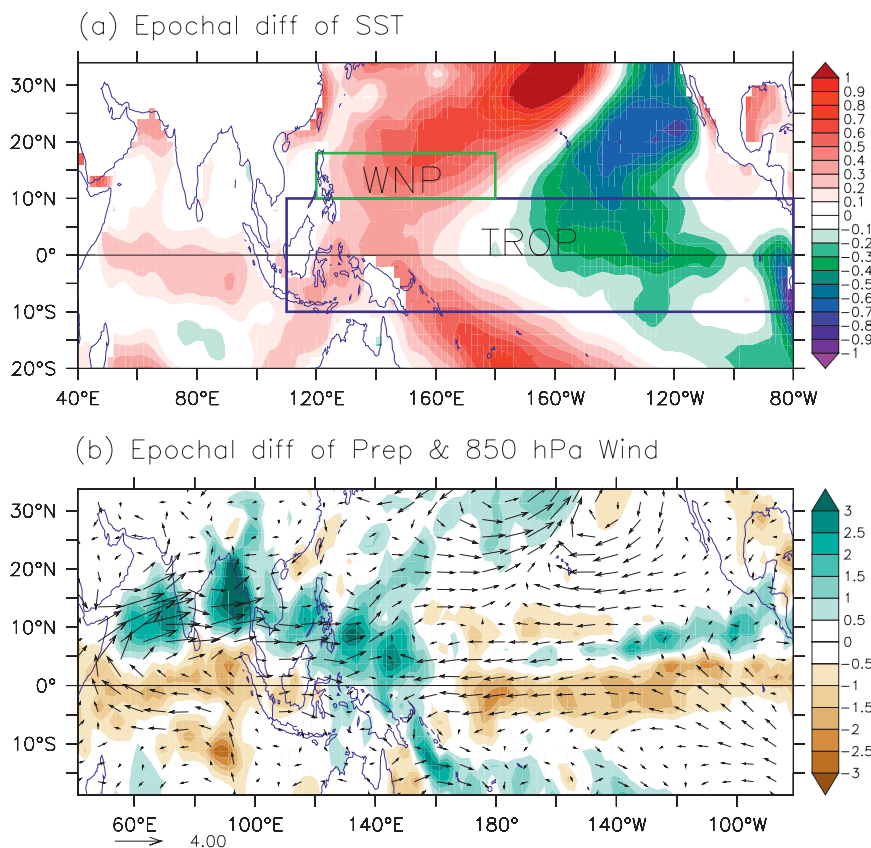


FIG. 4. Epochal differences of (a) SST ( $^{\circ}\text{C}$ ) and (b) precipitation (shading in  $\text{mm day}^{-1}$ ) and 850-hPa winds ( $\text{m s}^{-1}$ ) between post-1999 and pre-1999 in May. The designs of coupled model experiments are primarily based on the smoothed epochal SST difference in the tropical region [blue box in (a)] and the WNP [green box in (a)].

confirmed by using the Lepage test with a sample number of 10 (Lepage 1971; Yonetani 1992). The abrupt decadal shifts for these two indices are indeed detected at year 1999 with a 95% confidence level. The epochal differences (post-1999 – pre-1999) of precipitation and 850-hPa winds bear a resemblance to the trend patterns (Figs. 2a,b). However, within the short studied period, it cannot be discerned that this variability is one part of the trend or decadal-scale fluctuation. We will discuss this more in section 5.

Given the high correlation of these two indices ( $r = 0.83$  during 1979–2010), hereinafter we take the index defined by U850 as the ASMO index. To identify the driver controlling the ASMO change, we then plot the simultaneous correlation between the ASMO index and SST (Fig. 3a), which features a well-known La Niña-like pattern with SST warming in the WP and cooling in the equatorial central eastern Pacific (CEP). Meanwhile, a pronounced SST cooling appears in the northern IO (around 10°N) that mainly manifests a passive element of the enhanced wind speed. It is noteworthy that the

SST cooling is less significant using the precipitation-based ASMO index, but the Pacific shows a quite similar La Niña-like pattern (not shown).

Figure 3b illustrates that the ASMO index is significantly correlated with the zonal SST gradients in the tropical Pacific basin ( $r = 0.73$ ). Of particular interest is that a concurrent decadal shift of the zonal SST gradients is found in 1999 (Fig. 3b), and the epochal SST difference in May (post-1999 – pre-1999) does display a significant—“grand”—La Niña-like pattern (Fig. 4a). In summary, the ASMO change is closely linked to the tropical Pacific SST change not only on interannual time scales but also on decadal time scales.

#### *b. Contrasts of ASMO change in three regions: ArS, BoB, and SCS*

Since the ASMO index we used here covers large zonal domain from 50° to 120°E (Fig. 2), one may wonder whether this index can well represent the local variability at each subdomain. To answer this, we build three individual monsoon onset indices by using U850 in

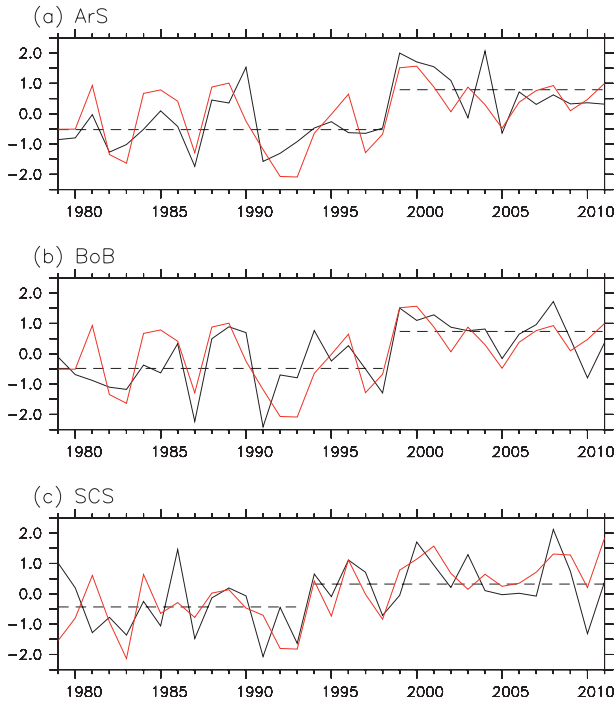


FIG. 5. Three individual monsoon onset indices (solid gray lines) obtained by using U850 averaged over each marginal sea: (a) Arabian Sea (ArS;  $5^{\circ}$ – $15^{\circ}$ N,  $50^{\circ}$ – $75^{\circ}$ E), (b) Bay of Bengal (BoB;  $5^{\circ}$ – $15^{\circ}$ N,  $80^{\circ}$ – $100^{\circ}$ E), and (c) South China Sea (SCS;  $5^{\circ}$ – $15^{\circ}$ N,  $110^{\circ}$ – $120^{\circ}$ E). The black dashed lines denote the mean value of these indices at each epoch separated by 1999, 1999, and 1994 for ArS, BoB, and SCS, respectively. The red lines in (a) and (b) are the normalized zonal SST gradients (blue box – green box in Fig. 3a), and the red line in (c) depicts the normalized SST in the WNP ( $10^{\circ}$ – $18^{\circ}$ N,  $135^{\circ}$ – $175^{\circ}$ E) in May.

May in three marginal seas: ArS ( $5^{\circ}$ – $15^{\circ}$ N,  $50^{\circ}$ – $75^{\circ}$ E), BoB ( $5^{\circ}$ – $15^{\circ}$ N,  $80^{\circ}$ – $100^{\circ}$ E), and SCS ( $5^{\circ}$ – $15^{\circ}$ N,  $110^{\circ}$ – $120^{\circ}$ E) (Fig. 5). These three indices are all significantly correlated with the ASMO index:  $r(\text{ArS}, \text{ASMO}) = 0.89$ ,  $r(\text{BoB}, \text{ASMO}) = 0.97$ , and  $r(\text{SCS}, \text{ASMO}) = 0.75$ . Meanwhile, these three indices are also interrelated:  $r(\text{ArS}, \text{BoB}) = 0.79$ ,  $r(\text{BoB}, \text{SCS}) = 0.77$ , and  $r(\text{ArS}, \text{SCS}) = 0.41$ . However, the correlation between ArS and SCS is relatively low, giving an indication of regional differences of monsoon variability. As shown in Fig. 5, the monsoon onset indices in the ArS and BoB exhibit an abrupt decadal shift at 1999, whereas the SCS has an evident decadal shift at 1994, which is in agreement with Kajikawa and Wang (2012). From this point of view, the mechanism resulting in the abrupt monsoon onset shift in the ArS is likely the same as for the BoB but different from that for the SCS.

By the same token, Fig. 6 portrays the simultaneous correlation map of these three indices with precipitation, 850-hPa winds, and SST. It is evident that

the monsoon onset indices in the ArS and BoB exhibit similar winds, precipitation, and SST patterns. Intensified precipitation and westerly wind anomaly extend from the ArS to the WNP with a northwest–southeast tilt structure, and the Pacific basin is characterized by a La Niña–like pattern together with suppressed precipitation and enhanced trades (Fig. 6). This pattern is similar with the epochal differences between post-1999 and pre-1999 (Fig. 4). By contrast, the pattern related to the SCS monsoon onset index mainly resembles a localized feature with strong cyclonic circulation and increased precipitation in the WNP, in spite of relatively weak zonal wind correlation in the northern IO (Fig. 6). The associated SST also differs: there is notable positive correlation in the WNP near the Philippine Sea and relatively weak negative correlation in the equatorial CEP. Meanwhile, the WNP SST near the Philippine Sea exhibits a robust warming shift at around 1994 (Fig. 5c) but the equatorial CEP does not (not shown). Therefore, we suggest that the significant monsoon onset shifts in the ArS and BoB are dominantly controlled by the abrupt increase of zonal SST gradients in the Pacific basin in 1999, but that in the SCS is mainly forced by the abrupt SST warming shift near the Philippine Sea in 1994 (Fig. 5).

The analysis outlined above demonstrates that the seasonal advance of ASM is synchronized with the decadal shift in the Pacific mean state. In the next section, we will use numerical models to explore the physical processes through which the Pacific mean state change alters the large-scale circulations in the WNP and IO as well as the advanced ASMO.

#### 4. Dynamics controlling the advanced ASMO

With the aid of a newly developed coupled model—POEM (Xiang et al. 2012)—and an intermediate atmospheric model (Wang and Li 1993), this section is devoted to addressing how the advanced ASMO is related to the Pacific mean state change. The purpose of using a coupled model is that air–sea coupling helps to establish better mean states (e.g., Fu et al. 2002) and variability (e.g., Wang et al. 2004) in the monsoon region, which is of particular importance in realistically reproducing the anomalous atmospheric responses.

##### a. Pacific-induced advanced ASMO in a coupled model

Five coupled model experiments are conducted and each has 20 ensembles (Table 1). As described in section 2, the first experiment is a fully coupled control run (CTRL) with annual mean SST correction in the equatorial Pacific and southeast Pacific. Figure 7

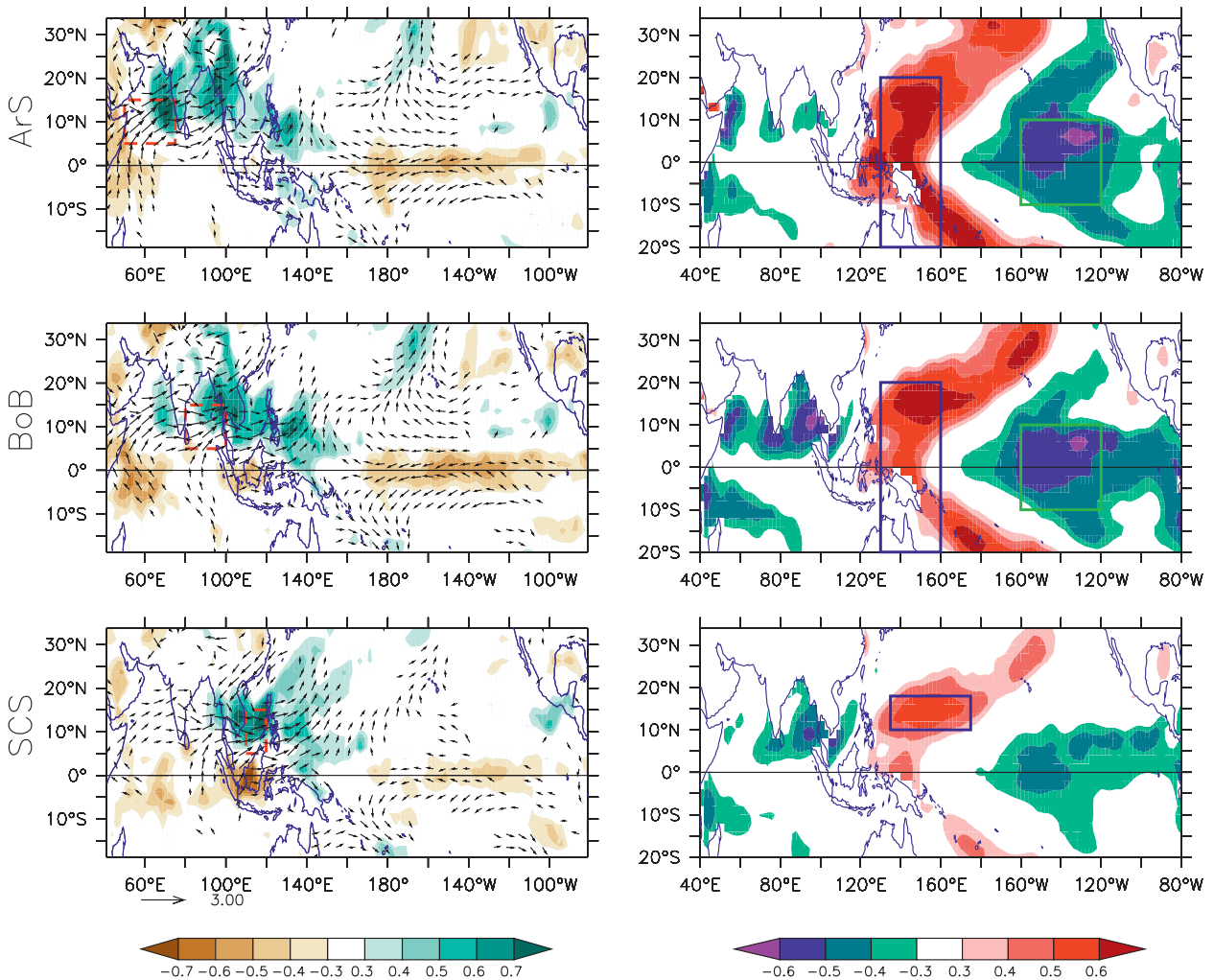


FIG. 6. (left) The simultaneous correlation map of three (ArS, BoB, SCS) monsoon onset indices with precipitation (shading) and 850-hPa winds (shown only when either the zonal or meridional wind correlation is  $>0.3$ ). (right) As at left, but for the correlation with SST. Three individual monsoon onset indices are defined by using U850 averaged over ArS ( $5^{\circ}$ – $15^{\circ}$ N,  $50^{\circ}$ – $75^{\circ}$ E), BoB ( $5^{\circ}$ – $15^{\circ}$ N,  $80^{\circ}$ – $100^{\circ}$ E), and SCS ( $5^{\circ}$ – $15^{\circ}$ N,  $110^{\circ}$ – $120^{\circ}$ E), respectively (red dashed boxes in the left panel).

depicts the observed and simulated climatological SST, precipitation, and 850-hPa winds. With respect to the monthly mean fields in May, POEM realistically captures the SST pattern but suffers serious precipitation and wind biases in the IO and WP (Fig. 7e). The simulated maximum precipitation remains straddling the equator of the IO together with weak westerly slightly to the north of the equator. This implies that the simulated ASMO in this coupled model is later in comparison to observations. Hence we further examine the model mean states averaged from 14 May to 13 June (Figs. 7c,f) and notice that the maximum westerly flow migrates northward to a latitude about  $5^{\circ}$ N in the IO, which is more in accordance with the observational monthly mean patterns in May. As

mentioned above, since the anomalous atmospheric response to SST forcing largely depends on the background mean state, hereafter the anomalous atmospheric responses relative to the CTRL are based on the simulations averaged from 14 May to 13 June (as May mean states).

The designs of the following sensitivity experiments are primarily based on the epochal SST difference (post-1999 – pre-1999) in May as shown in Fig. 4a. Although the most pronounced SST change appears in the subtropical North Pacific with strong SST warming to the west and SST cooling to the east, the precipitation and circulation changes are usually more sensitive to SST change in the tropical regions. In particular, we emphasize the SST change in two regions, the

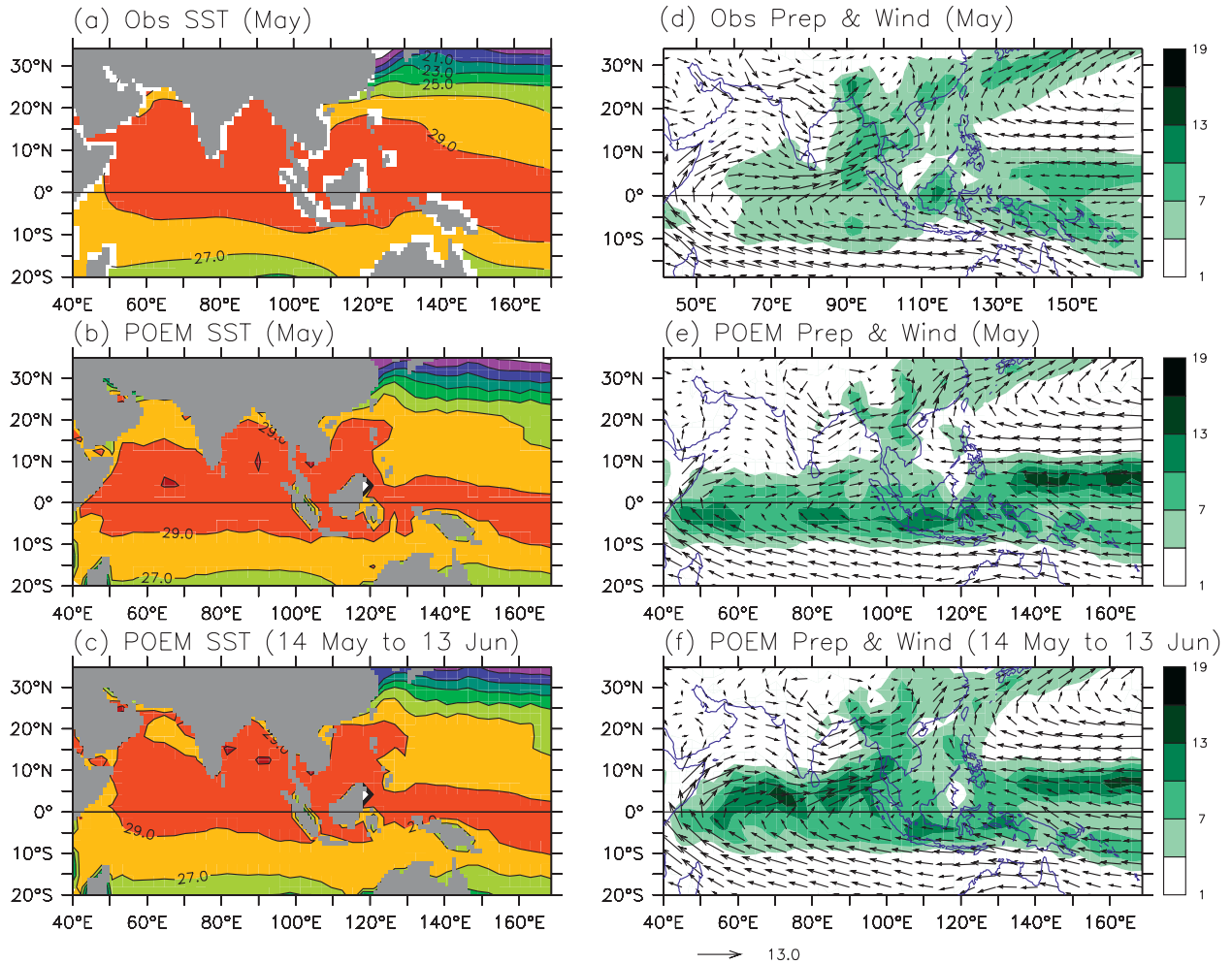


FIG. 7. (left) Climatological SST ( $^{\circ}\text{C}$ ) from (a) observations in May, (b) POEM in May, and (c) POEM from 14 May to 13 June. (right), As at left, but for precipitation (shading in  $\text{mm day}^{-1}$ ) and 850-hPa winds (vectors in  $\text{m s}^{-1}$ ).

tropical Pacific ( $10^{\circ}\text{S}$ – $10^{\circ}\text{N}$ ,  $110^{\circ}\text{E}$ – $80^{\circ}\text{W}$ ) and the WNP ( $10^{\circ}$ – $18^{\circ}\text{N}$ ,  $120^{\circ}\text{E}$ – $180^{\circ}$ ) (Fig. 4a). Therefore, the first sensitivity experiment (referred to as TROP) employs a constant SST nudging to the SST tendency equation in the tropical Pacific [contours in Fig. 8a,  $^{\circ}\text{C (5 day)}^{-1}$ ] from 1 January (Table 1), and the other regions are fully coupled. The initial condition for the sensitivity experiment adopts the same initial condition from the CTRL run for each year (ensemble). In comparison to the observational epochal difference (Fig. 4a), the SST nudging pattern in TROP is spatially smoothed and modified to some extent. For example, the SST cooling nudging in the CEP is reduced but the warming nudging in the south WP is amplified (contours in Fig. 8a) because air–sea coupling may amplify or reduce the imposed SST nudging signal.

As expected, the resultant SST difference (TROP minus CTRL) exhibits pronounced SST warming in

the equatorial WP and SST cooling in the equatorial CEP (shading in Fig. 8a). The coherent suppressed precipitation is residing in the equatorial CEP and tropical IO south to the equator (Fig. 8b). By contrast, conspicuously enhanced precipitation and westerly flow extend from the WP to the northern IO. This model difference generally reproduces the epochal difference pattern from observation, despite the precipitation and zonal wind anomalies tend to be more equatorially trapped especially in the ArS (Fig. 8b). The above experiments support our speculation that the La Niña-like pattern in the Pacific basin favors the advanced ASMO.

To further identify the individual effect of the SST warming in the WP and SST cooling in the CEP on the advanced ASMO, we made two more sensitivity experiments, called TROP\_warm, with SST warming nudging only in the equatorial WP, and TROP\_cold,

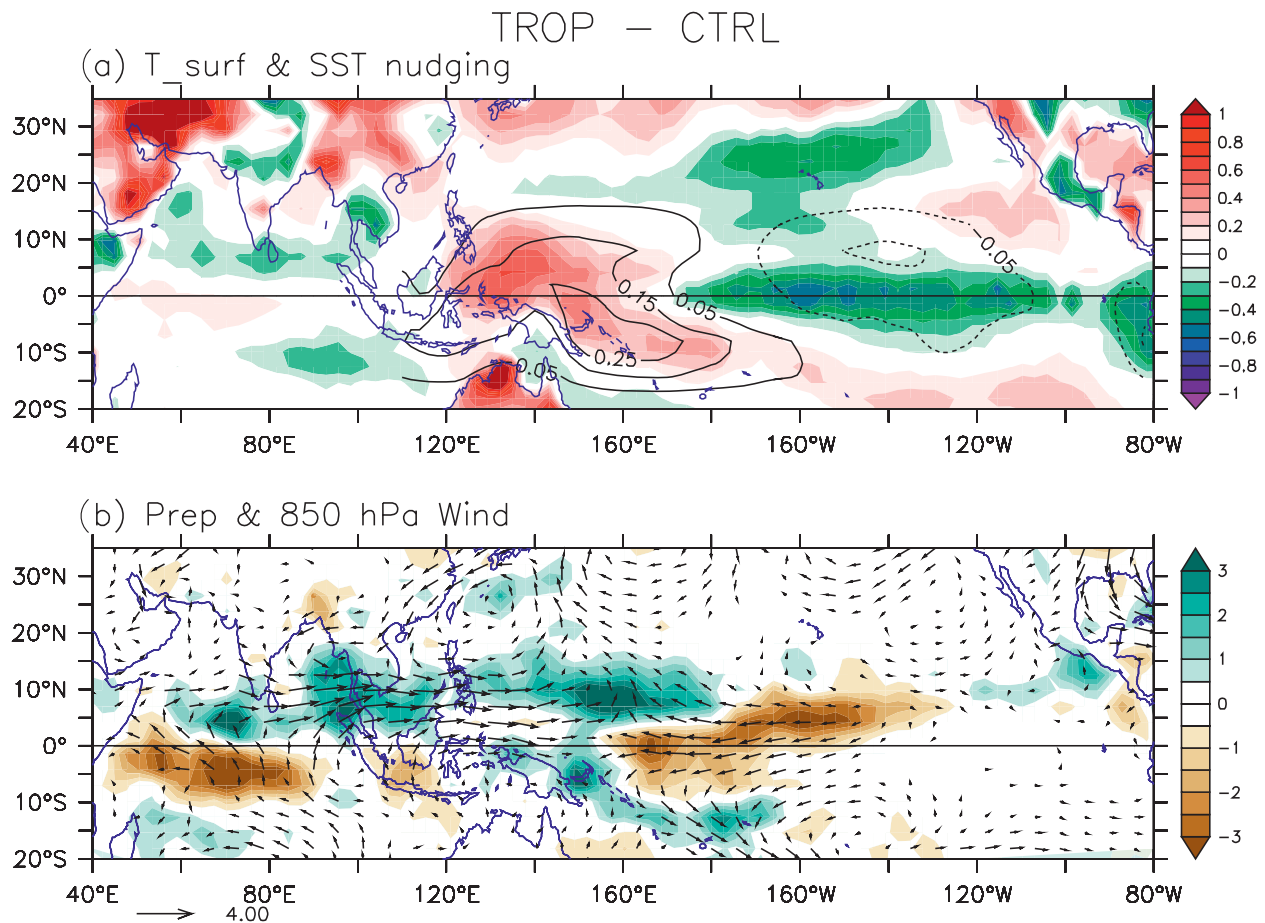


FIG. 8. (a) The imposed SST nudging pattern [contours in  $^{\circ}\text{C} (5 \text{ days})^{-1}$ ] in the POEM coupled model, and the combined ensemble mean SST and land surface air temperature differences (shading in  $^{\circ}\text{C}$ ) between the experiments TROP and CTRL. (b) Ensemble mean precipitation (shading in  $\text{mm day}^{-1}$ ) and 850-hPa winds ( $\text{m s}^{-1}$ ) differences between TROP and CTRL. All variables are averaged from 14 May to 13 June.

with SST cooling nudging only in the CEP (Table 1). The anomalous fields of these two experiments compared with CTRL are illustrated in Fig. 9. Interestingly, both of these two experiments can produce enhanced precipitation and westerly winds in the northern IO. The major difference of these two experiments is that the TROP<sub>warm</sub> induces strong suppressed precipitation over the equatorial IO, which may facilitate the advanced monsoon onset over the ArS and BoB (Fig. 9b). It is concluded that the decadal SST warming in the tropical WP and the SST cooling in the CEP cooperatively determine the advanced ASMO over the ArS and BoB.

Another feature worthy of note is that the surface air temperature becomes noticeably warmer in the land region over the Middle East for these three experiments (TROP, TROP<sub>warm</sub>, TROP<sub>cold</sub>; Figs. 8a, 9a, 9c), which increases the land–sea heat contrast so as to favor

the monsoon onset over the ArS. This is consistent with the observed land–sea heat contrast change (Wang et al. 2012b). Here we argue that this surface temperature warming over the Middle East mainly acts as a consequence of the above-normal precipitation over the northern IO through modulating the Hadley circulation, with its root cause residing in the Pacific mean state change.

The abrupt SST warming in the Philippine Sea after 1994 is claimed to hold the key for the advanced monsoon onset in the SCS (Fig. 4a). To illustrate this point, another coupled model experiment (WNP<sub>warm</sub>) is conducted with imposed SST warming nudging near the Philippine Sea (contours in Fig. 10a). Clearly, the SST warming near the Philippine Sea generates a strong cyclonic circulation in the WNP, accompanied by prominent westerly winds in the SCS. Meanwhile, this WNP SST warming does not produce considerable

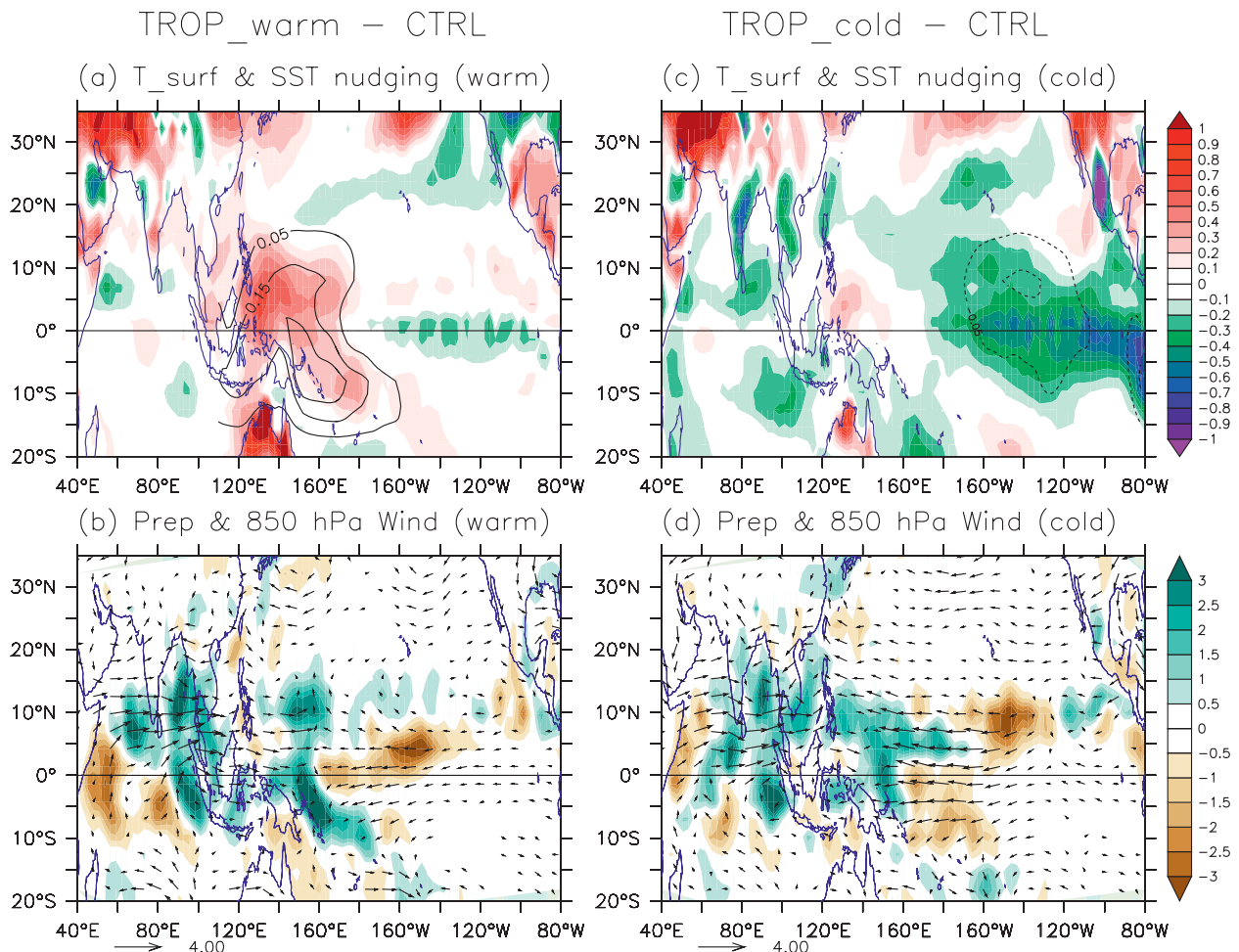


FIG. 9. (left) As in Fig. 8, but for the differences between TROP\_warm (warm SST nudging in the equatorial WP) and CTRL. (right) Differences between TROP\_cold (cold SST nudging in the CEP) and CTRL.

precipitation and westerly anomalies in the northern IO. This well accounts for the fact that the abrupt monsoon onset shift in the SCS is different from that in the ArS and BoB. However, we do not rule out a possible role for CEP SST change in regulating the SCS monsoon onset. The coupled model experiment (Fig. 9d) illustrates that the CEP cooling does favor the advanced monsoon onset in SCS. But again, the WNP SST warming is argued to dominate over the CEP cooling in determining the abrupt monsoon onset over the SCS at 1994, through exciting a cyclonic circulation and intensification of the biweekly oscillation in the Philippine Sea and SCS (Kajikawa and Wang 2012).

Given the rather equatorially symmetric SST change in the Pacific basin (Fig. 4a), it poses the following question: Why are the precipitation and circulation changes asymmetric in the IO and WP? Understanding this is essential to unveil the physical mechanisms

determining the abrupt monsoon onset shift, particularly for the ArS and BoB.

#### *b. Role of asymmetric mean states in the advanced ASMO*

In the previous subsection, we have performed coupled model experiments to document the critical role of the Pacific SST change in regulating the ASMO. However, the coupled model results do not provide direct evidence as to why the precipitation and winds responses are asymmetric about the equator, particularly with strongly enhanced precipitation and westerly winds confining in the northern IO and WNP. In this section, emphasis is placed on understanding the physical processes that establish the connection between Pacific mean state change and the advanced ASMO. Here we argue that the asymmetric basic mean states in May, especially the vertical zonal wind shear and moisture in

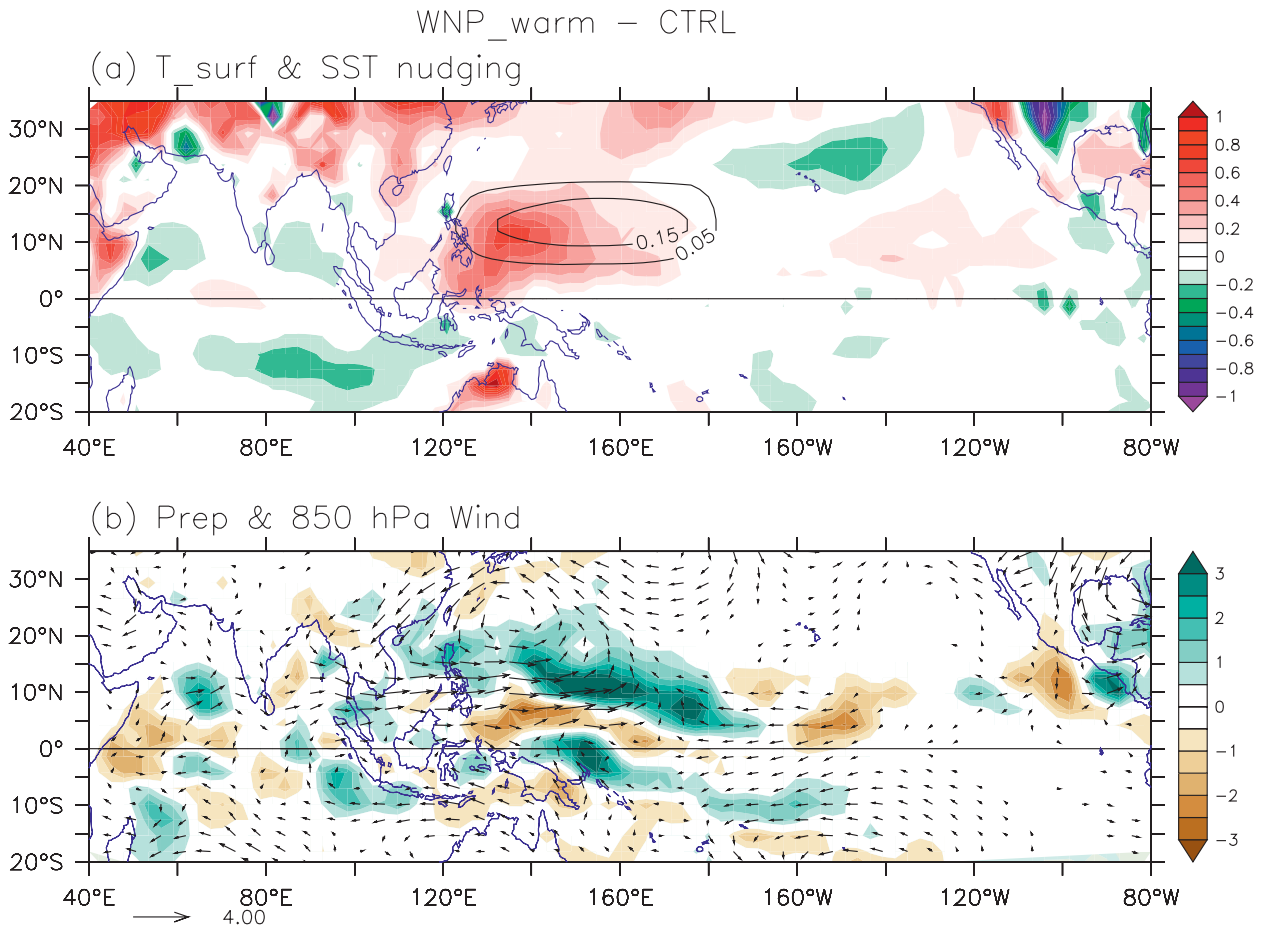


FIG. 10. As in Fig. 8, but for the differences between the experiments WNP\_warm (warm SST nudging in the WNP) and CTRL.

the IO and WNP, play prime roles in causing the asymmetric atmospheric response as well as the advanced ASMO in the ArS and BoB.

Through the local and remote forcing effects, both the WP SST warming and CEP SST cooling contribute to the intensified convection near the southeast of Philippine Sea. The abnormally intensified convection near the southeast of Philippine Sea then facilitates the enhanced precipitation and westerly wind anomalies in the SCS and northern IO associated with the westward emanation of Rossby waves and their strong interactions with background mean states.

Investigation of the background mean states is instrumental in clarifying the basic mechanisms and feedbacks at play. Wang and Xie (1996) demonstrated that background mean easterly vertical wind shear tends to weaken the upper-level Rossby response but strengthen the low-level Rossby wave response. This has been proposed to be vital for the rapid development of Indian Ocean dipole (IOD) during boreal summer (Xiang et al. 2011). In May, pronounced

meridional asymmetry of mean vertical shear occurs in the IO and WP with strong easterly shear to the north of the equator (Fig. 11a), so it is anticipated that such an equatorial asymmetry of the mean vertical shear favors the amplification of low-level Rossby waves response, especially for the Northern Hemisphere branch. Meanwhile, the mean moisture also exhibits robust meridional asymmetry with more moisture in the Northern Hemisphere (Fig. 11b). When the cyclonic perturbations propagate to the SCS and northern IO from the WNP (near 5°N, 140°E), the perturbations tend to develop rapidly because the mean state-induced strengthened low-level Rossby waves give rise to prominent boundary moisture convergence, which then feeds back to the anomalous deep convection (Xie and Wang 1996). Therefore, the meridional asymmetry of mean easterly shear and moisture distribution is conducive to the rapid development of anomalous perturbation to the north of the equator.

The robustness of the above argument can be established by comparing two experiments with an

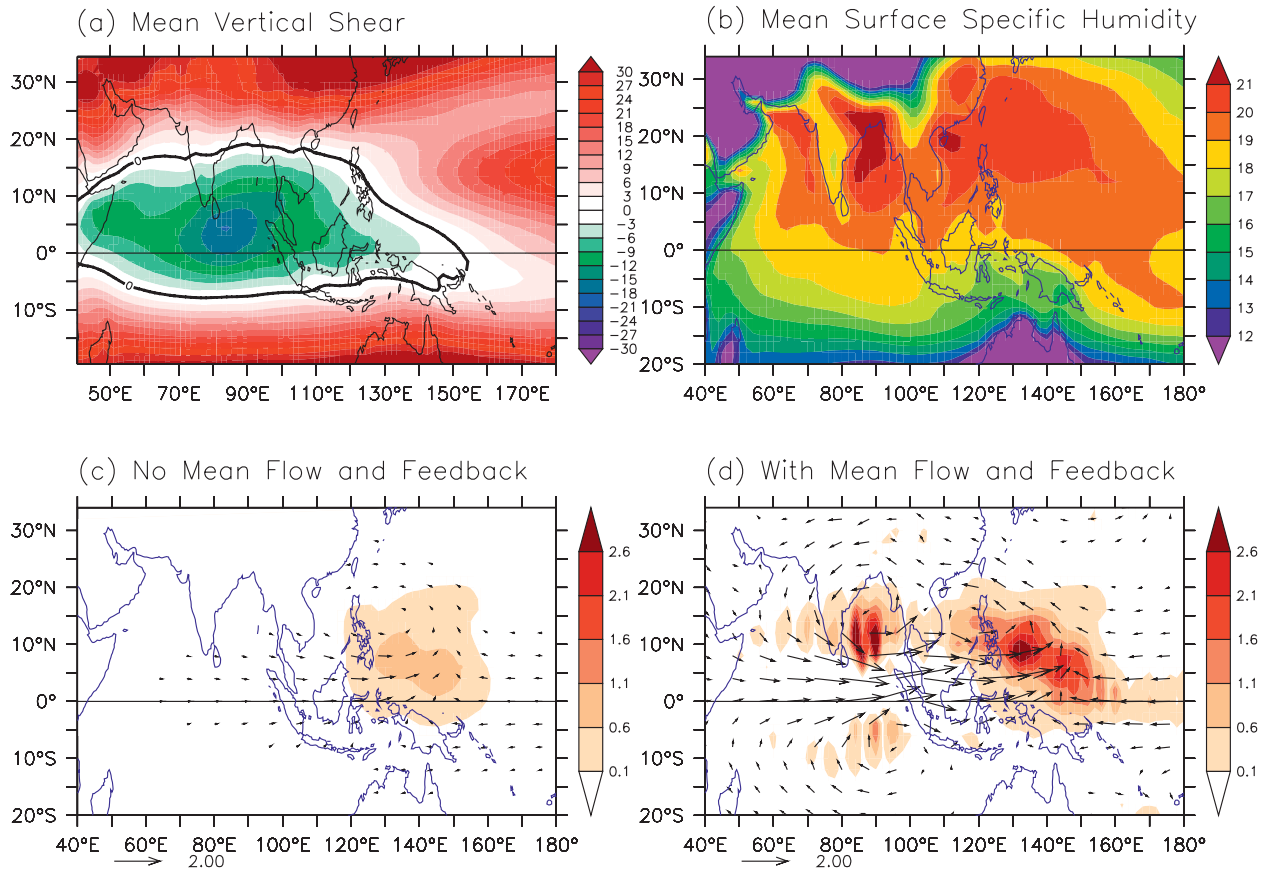


FIG. 11. (a) Climatological vertical shear of zonal winds ( $\text{m s}^{-1}$ ) defined by the zonal winds difference between 200 and 850 hPa in May. (b) Climatological surface (2 m) specific humidity in May ( $\text{g kg}^{-1}$ ). (c) Low-level wind response (vectors in  $\text{m s}^{-1}$ ) to a prescribed midtropospheric heating in the WP (shading in  $\text{K day}^{-1}$ ) by using an intermediate 2½-layer atmospheric model. In this experiment there are no background mean flow and feedback. (d) As in (c), but with climatological mean flow and moisture in May, which allows the feedback processes to be effective.

intermediate 2.5-layer atmospheric model (Wang and Li 1993). A specified midtropospheric heating is imposed in the WP ( $5^{\circ}\text{S}$ – $20^{\circ}\text{N}$ ,  $120^{\circ}$ – $160^{\circ}\text{E}$ ) (shading in Fig. 11c). Note that the maximum of the heating lies slightly to the north of the equator, which is constructed based on the epochal precipitation difference as shown in Fig. 4b. In the absence of background mean flow and boundary moisture feedback, the atmospheric wind response is weak and constrained in the equatorial WP (Fig. 11c). However, the atmospheric response differs substantially from the case with prescribed background mean flow and moisture (Fig. 11d). The gross features resemble the observed atmospheric response with dramatically increased response over the WNP, SCS, and the northern IO. Compared with the observed pattern, the major discrepancy is that the westerly flow is more equatorially trapped (Fig. 11d). This can be explained by the fact that the model does not produce negative heating over the equatorial IO

even with apparent boundary divergence there. Hence, the model results lend support to the assertion that the meridional contrast of mean states (vertical shear and moisture) constitutes the optimal configuration for the amplification of the perturbation in the Northern Hemisphere that results in the advanced ASMO.

### 5. Nature of the recent advance of ASMO

As discussed in section 3, both the trend variability and abrupt decadal shift are significant for the ASMO in recent three decades (Figs. 2c,d). It begs the question of whether the ASMO change is ascribable to natural decadal variability or anthropogenic forcing. In the earlier part of this study, we focus on a relatively short period that cannot address this question. Here we extend it to the middle of twentieth century with the data comprising reanalysis (NCEP1, NCEP2, ERA-40) and observational (WASWind) datasets.

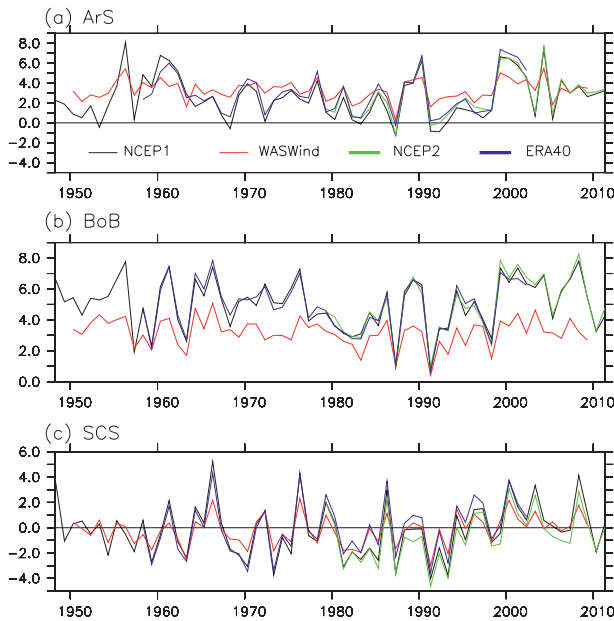


FIG. 12. (top to bottom) Three (ArS, BoB, SCS) monsoon onset indices using 850-hPa reanalysis (NCEP1, NCEP2, ERA-40) and 10-m observational (WASWind) winds. The definitions of these three indices are based on zonal wind averaged over ArS ( $5^{\circ}$ – $15^{\circ}$ N,  $50^{\circ}$ – $75^{\circ}$ E), BoB ( $5^{\circ}$ – $15^{\circ}$ N,  $80^{\circ}$ – $100^{\circ}$ E), and SCS ( $5^{\circ}$ – $15^{\circ}$ N,  $110^{\circ}$ – $120^{\circ}$ E).

As shown in Fig. 12, the three monsoon onset indices (ArS, BoB, and SCS) do have consistent and robust shifts in the mid-to-late 1990s, although the magnitude of 10-m WASWind has some difference with others. What is the most important is that they do not attain apparent trends from the middle of the twentieth century. It strongly suggests that the advanced ASMO in recent decades is attributed to natural decadal variability. Meanwhile, we can also notice that the zonal winds become weaker after the late 1970s to the mid-1990s compared with the period between 1960s and 1970s (Fig. 12), indicating a delayed ASMO onset that is possibly linked to the well-known decadal shift in the late 1970s.

Meanwhile, Zhang et al. (2012) diagnosed the ASMO based on the climate models that participated in the IPCC Fourth Assessment Report (AR4), and found that the majority of the models features delayed onset over the tropical IO, Maritime Continent, and Indochina Peninsula under a warmed climate, especially when the ocean warming signature resembles an El Niño-like pattern. This is consistent with our argument that La Niña-like mean states are conducive to an advanced ASMO, and vice versa. Based on all the above evidence, we advocate that the considerable advance of the ASMO in the recent three decades mainly arises from

natural decadal variability rather than from anthropogenic forcing.

## 6. Summary and discussion

This study is motivated by the fact that the ASMO has been advanced in recent three decades (Kajikawa et al. 2012). In this paper, we use observational data and numerical models to elaborate on the mechanisms controlling the advanced ASMO. It is revealed that the advanced ASMO owes its existence to the mean state change in the Pacific basin characterized by a “grand” La Niña-like pattern. The warm SST in the WP and cold SST in the CEP both contribute to the advanced ASMO through a positive feedback mechanism that involves the interaction between atmospheric waves and the meridional asymmetric mean states. The Pacific mean state change and associated intensification of convection over the WP (Fig. 4b) also produce an east–west heating contrast between the WP and IO. Kucharski et al. (2011) suggested that the upper-level divergence (negative velocity potential) in the WP is partly responsible for the intensification of the South Asia high (positive streamfunction) (Fig. 13). This upper-level high and easterly jet may further feed back to strengthen the convection, particularly over the BoB, by inducing a secondary circulation (Hoskins and Wang 2006). But this effect should be secondary in driving the advance of ASMO.

This study sheds light on the importance of the atmospheric wave dynamics and its interaction with the background mean states, and provides dynamical insights about the role of the Pacific mean state change in regulating the ASMO. In reality, the monsoon onset in the ArS and BoB exhibits a clear abrupt shift at 1999, while the SCS monsoon onset is observed to shift at 1994. We have demonstrated that the decadal shifts of monsoon onset in the ArS and BoB are primarily controlled by the equatorial zonal SST gradients in the Pacific basin, while that for the SCS monsoon onset is mainly determined by the SST variability near the Philippine Sea.

This “grand” La Niña-like mean state change in the recent decades has profound implications for understanding some important climate issues. For example, it is strongly coupled to the global monsoon intensification (Wang et al. 2012a) and largely responsible for the more frequent occurrence of central Pacific El Niño, especially after the late 1990s (Xiang et al. 2013). Based on this study, we advocate that the Pacific mean state change acts as the root cause for the intensification of tropical cyclone in the ArS after 1997 (Wang et al. 2012b). However, what triggers and maintains this La Niña-like mean state change requires further investigations.

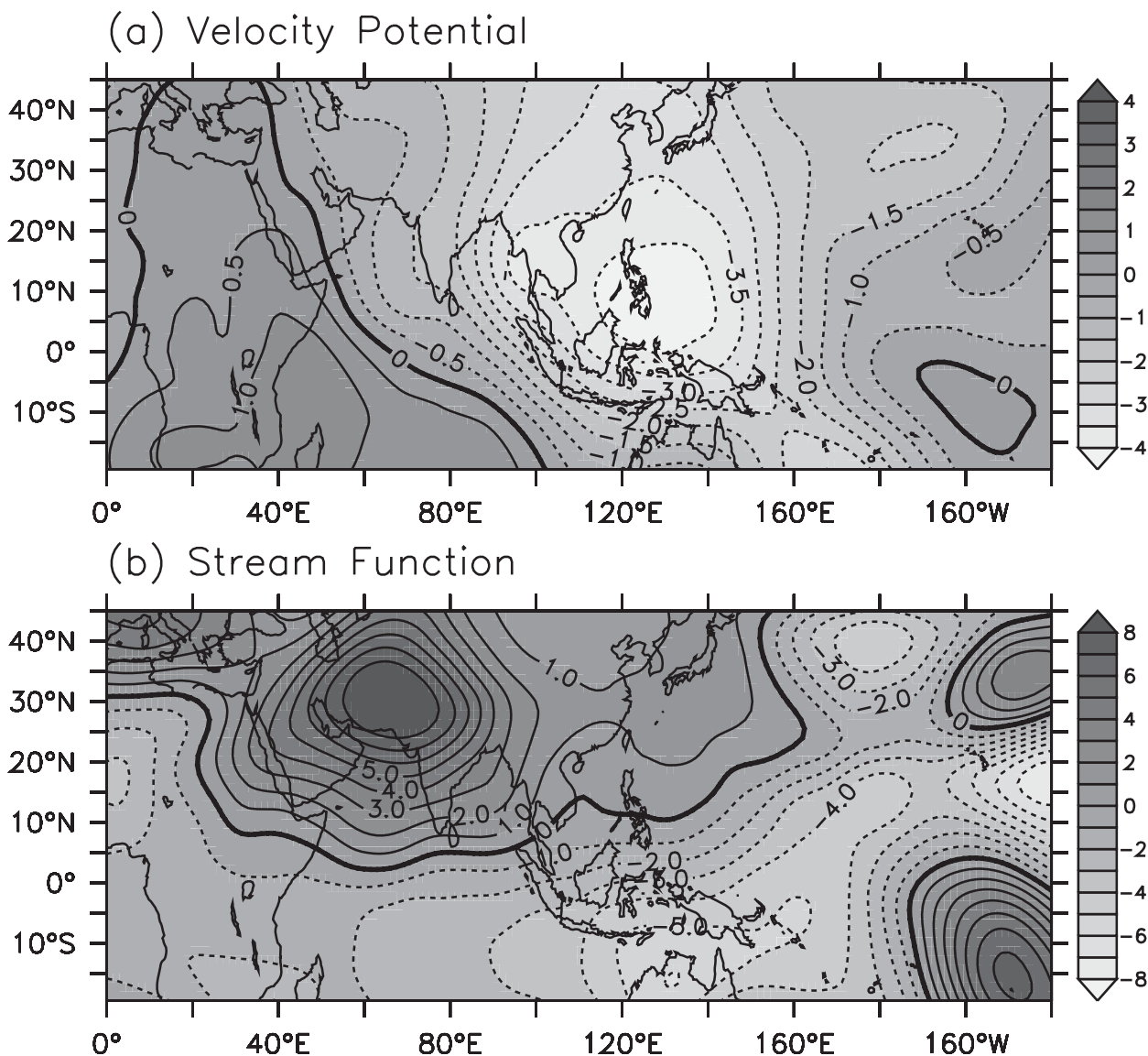


FIG. 13. The epochal differences of (a) 200-hPa velocity potential ( $10^6 \text{ m}^2 \text{ s}^{-1}$ ) and (b) 200-hPa streamfunction ( $10^6 \text{ m}^2 \text{ s}^{-1}$ ) between 1999–2011 and 1979–98 in May by using ERA-Interim datasets.

**Acknowledgments.** The authors are grateful to Dr. Renguang Wu, the editor of *Journal of Climate*, and four reviewers for their helpful comments. We also thank Dr. Fei Liu for helping set up the intermediate atmospheric model, Dr. June-Yi Lee's comments on this paper, and Dr. Hiroki Tokinaga for providing the WASWind data. This work has been supported by the Climate Dynamics Program of the National Science Foundation under Award AGS-1005599, and by the APEC Climate Center. The authors acknowledge partial support from the International Pacific Research Center, which is sponsored by JAMSTEC, NASA (NNX07AG53G), and NOAA (NA09OAR4320075).

#### REFERENCES

- Adler, R. F., and Coauthors, 2003: The version-2 Global Precipitation Climatology Project (GPCP) monthly precipitation analysis (1979–present). *J. Hydrometeorol.*, **4**, 1147–1167.
- Dee, D. P., and Coauthors, 2011: The ERA-Interim reanalysis: Configuration and performance of the data assimilation system. *Quart. J. Roy. Meteor. Soc.*, **137**, 553–597.
- Ding, Q., and B. Wang, 2005: Circumglobal teleconnection in the Northern Hemisphere summer. *J. Climate*, **18**, 3483–3505.
- , —, J. M. Wallace, and G. Branstator, 2011: Tropical–extratropical teleconnections in boreal summer: Observed interannual variability. *J. Climate*, **24**, 1878–1896.
- Fu, X., B. Wang, and T. Li, 2002: Impacts of air–sea coupling on the simulation of the mean Asian summer monsoon in the ECHAM4 model. *Mon. Wea. Rev.*, **130**, 2889–2904.

- Gill, A. E., 1980: Some simple solutions for heat-induced tropical circulation. *Quart. J. Roy. Meteor. Soc.*, **106**, 447–462.
- Hoskins, B., and B. Wang, 2006: Large-scale atmospheric dynamics. *The Asian Monsoon*, B. Wang, Ed., Springer/Praxis, 357–415.
- Hsu, P., T. Li, and B. Wang, 2011: Trends in global monsoon area and precipitation over the past 30 years. *Geophys. Res. Lett.*, **38**, L08701, doi:10.1029/2011GL046893.
- , —, J.-J. Luo, H. Murakami, A. Kitoh, and M. Zhao, 2012: Increase of global monsoon area and precipitation under global warming: A robust signal? *Geophys. Res. Lett.*, **39**, L06701, doi:10.1029/2012GL051037.
- Hu, Z.-Z., 1997: Interdecadal variability of summer climate over East Asia and its association with 500-hPa height and global sea surface temperature. *J. Geophys. Res.*, **102** (D16), 19 403–19 412.
- Kajikawa, Y., and B. Wang, 2012: Interdecadal change of the South China Sea summer monsoon onset. *J. Climate*, **25**, 3207–3218.
- , T. Yasunari, S. Yoshida, and H. Fujinami, 2012: Advanced Asian summer monsoon onset in recent decades. *Geophys. Res. Lett.*, **39**, L03803, doi:10.1029/2011GL050540.
- Kalnay, E., and Coauthors, 1996: The NCEP/NCAR 40-Year Reanalysis Project. *Bull. Amer. Meteor. Soc.*, **77**, 437–471.
- Kanamitsu, M., W. Ebisuzaki, J. Woollen, S. K. Yang, J. J. Hnilo, M. Fiorino, and G. L. Potter, 2002: NCEP-DOE AMIP-II Reanalysis (R-2). *Bull. Amer. Meteor. Soc.*, **83**, 1631–1643.
- Kim, K.-M., and K.-M. Lau, 2001: Dynamics of monsoon-induced biennial variability in ENSO. *Geophys. Res. Lett.*, **28**, 315–318.
- Kirtman, B. P., and J. Shukla, 2000: Influence of the Indian summer monsoon on ENSO. *Quart. J. Roy. Meteor. Soc.*, **126**, 213–239.
- Kucharski, F., A. Bracco, R. Barimalala, and J. H. Yoo, 2011: Contribution of the east–west thermal heating contrast to the South Asian monsoon and consequences for its variability. *Climate Dyn.*, **37**, 721–735, doi:10.1007/s00382-010-0858-3.
- Kumar, K. K., B. Rajagopalan, M. Hoerling, G. Bates, and M. Cane, 2006: Unraveling the mystery of Indian monsoon failure during El Niño. *Science*, **314**, 115–119.
- Kwon, M., J.-G. Jhun, and K.-J. Ha, 2007: Decadal change in East Asian summer monsoon circulation in the mid-1990s. *Geophys. Res. Lett.*, **34**, L21706, doi:10.1029/2007GL031977.
- Lau, K.-M., and S. Yang, 1997: Climatology and interannual variability of the Southeast Asian summer monsoon. *Adv. Atmos. Sci.*, **14**, 141–162.
- Lee, J.-Y., and B. Wang, 2013: Future change of global monsoon in the CMIP5. *Climate Dyn.*, doi:10.1007/s00382-012-1564-0, in press.
- , and Coauthors, 2010: How are seasonal prediction skills related to models' performance on mean state and annual cycle? *Climate Dyn.*, **35**, 267–283.
- , B. Wang, Q. Ding, K.-J. Ha, J.-B. Ahh, A. Kumar, B. Stern, and O. Alves, 2011: How predictable is the Northern Hemisphere summer upper-tropospheric circulation? *Climate Dyn.*, **37**, 1189–1203.
- Lepage, Y., 1971: A combination of Wilcoxon's and Ansari-Bradley's statistics. *Biometrika*, **58**, 213–217.
- Lindzen, R. S., and S. Nigam, 1987: On the role of sea surface temperature gradients in forcing low-level winds and convergence in the tropics. *J. Atmos. Sci.*, **44**, 2418–2436.
- Murakami, T., and J. Matsumoto, 1994: Summer monsoon over the Asian continent and western North Pacific. *J. Meteor. Soc. Japan*, **72**, 719–745.
- Ramage, C. S., 1972: *Monsoon Meteorology*. Academic Press, 296 pp.
- Roeckner, E., and Coauthors, 1996: The atmospheric general circulation model ECHAM-4: Model description and simulation of present-day climate. Max Planck Institute for Meteorology Rep. 218, 90 pp.
- Smith, R. D., J. K. Dukowicz, and R. C. Malone, 1992: Parallel ocean general circulation modeling. *Physica*, **60**, 38–61.
- Smith, T. M., R. W. Reynolds, T. C. Peterson, and J. Lawrimore, 2008: Improvements to NOAA's historical merged land–ocean surface temperature analysis (1880–2006). *J. Climate*, **21**, 2283–2296.
- Tanaka, M., 1992: Intraseasonal oscillation and the onset and retreat dates of the summer monsoon over the east, southeast and western North Pacific region using GMS high cloud amount data. *J. Meteor. Soc. Japan*, **70**, 613–629.
- Tao, S., and L. Chen, 1987: A review of recent research on the East Asian summer monsoon in China. *Monsoon Meteorology*, C.-P. Chang and T. N. Krishnamurti, Eds., Oxford University Press, 60–92.
- Tokina, H., and S.-P. Xie, 2011: Wave- and Anemometer-Based Sea Surface Wind (WASWind) for climate change analysis. *J. Climate*, **24**, 267–285.
- Uppala, S. M., and Coauthors, 2005: The ERA-40 Re-Analysis. *Quart. J. Roy. Meteor. Soc.*, **131**, 2961–3012.
- Valcke, S., A. Caubel, D. Declat, and L. Terry, 2003: OASIS3: Ocean–Atmosphere–Sea Ice–Soil user's guide. CERFACS Tech. Rep. TR/CMGC/03/69, 57 pp.
- Wang, B., and T. Li, 1993: A simple tropical atmospheric model of relevance to short-term climate variations. *J. Atmos. Sci.*, **50**, 260–284.
- , and X. Xie, 1996: Low-frequency equatorial waves in vertically sheared zonal flow. Part I: Stable waves. *J. Atmos. Sci.*, **53**, 449–467.
- , and LinHo, 2002: Rainy season of the Asian–Pacific summer monsoon. *J. Climate*, **15**, 386–398.
- , R. Wu, and X. Fu, 2000: Pacific–East Asia teleconnection: How does ENSO affect East Asian climate? *J. Climate*, **13**, 1517–1536.
- , I.-S. Kang, and J.-Y. Lee, 2004: Ensemble simulations of Asian–Australian monsoon variability by 11 AGCMs. *J. Climate*, **17**, 803–818.
- , and Coauthors, 2009: Advance and prospectus of seasonal prediction: Assessment of APCC/CliPAS 14-model ensemble retrospective seasonal prediction (1980–2004). *Climate Dyn.*, **33**, 93–117.
- , J. Liu, H.-J. Kim, P. J. Webster, and S.-Y. Yim, 2012a: Recent change of global monsoon precipitation (1979–2008). *Climate Dyn.*, **39**, 1123–1135, doi:10.1007/s00382-011-1266-z.
- , S. Xu, and L. Wu, 2012b: Intensified Arabian Sea tropical storms. *Nature*, **489**, E1–E2, doi:10.1038/nature11470.
- Webster, P. J., and S. Yang, 1992: Monsoon and ENSO: Selectively interactive system. *Quart. J. Roy. Meteor. Soc.*, **118**, 877–926.
- Woodward, W. A., and H. L. Gray, 1993: Global warming and the problem of testing for trend in time series data. *J. Climate*, **6**, 953–962.
- Wu, R., and B. Wang, 2001: Multi-stage onset of the summer monsoon over the western North Pacific. *Climate Dyn.*, **17**, 277–289.
- Xiang, B., W. Yu, T. Li, and B. Wang, 2011: The critical role of the boreal summer mean state in the development of the IOD. *Geophys. Res. Lett.*, **38**, L02710, doi:10.1029/2010GL045851.
- , B. Wang, Q. Ding, F.-F. Jin, X. Fu, and H.-J. Kim, 2012: Reduction of the thermocline feedback associated with mean SST bias in ENSO simulation. *Climate Dyn.*, **39**, 1413–1430, doi:10.1007/s00382-011-1164-4.

- , ——, and T. Li, 2013: A new paradigm for the predominance of standing central Pacific warming after the late 1990s. *Climate Dyn.*, doi:10.1007/s00382-012-1427-8, in press.
- Xie, X., and B. Wang, 1996: Low-frequency equatorial waves in vertically sheared zonal flows. Part II: Unstable waves. *J. Atmos. Sci.*, **53**, 3589–3605.
- Yonetani, T., 1992: Discontinuous changes of precipitation in Japan after 1900 detected by the Lepage test. *J. Meteor. Soc. Japan*, **70**, 95–104.
- Yu, W., K. Li, J. Shi, L. Liu, H. Wang, and Y. Liu, 2012a: The onset of the monsoon over the Bay of Bengal: The year-to-year variations. *Atmos. Oceanic Sci. Lett.*, **5**, 342–347.
- , J. Shi, L. Liu, K. Li, Y. Liu, and H. Wang, 2012b: The onset of the monsoon over the Bay of Bengal: The observed common features for 2008–2011. *Atmos. Oceanic Sci. Lett.*, **5**, 314–318.
- Zhang, H., P. Liang, A. Moise, and L. Hanson, 2012: Diagnosing potential changes in Asian summer monsoon onset and duration in IPCC AR4 model simulations using moisture and wind indices. *Climate Dyn.*, **39**, 2465–2486, doi:10.1007/s00382-012-1289-0.
- Zhou, T., L. Zhang, and H. Li, 2008: Changes in global land monsoon area and total rainfall accumulation over the last half century. *Geophys. Res. Lett.*, **35**, L16707, doi:10.1029/2008GL034881.